Rapid communication

High-pressure synthesis and single-crystal structure refinement of gadolinium holmium silicate hydroxyapatite $Gd_{4.33}Ho_{4.33}(SiO_4)_6(OH)_2$

Chao Wang[a], Xiaoyang Liu[a,*], M.E. Fleet[b], Shouhua Feng[a], Ruren Xu[a]

[a]*State Key Laboratory of Inorganic Synthesis and Preparative Chemistry, College of Chemistry, Jilin University, 2699 Qianjin Street, Changchun 130012, PR China*
[b]*Department of Earth Sciences, University of Western Ontario, London, Ont., Canada N6A 5B7*

Abstract

Single crystals of gadolinium holmium silicate hydroxyapatite $Gd_{4.33}Ho_{4.33}(SiO_4)_6(OH)_2$ have been synthesized at 2.0 GPa and 1450 °C using a piston-cylinder-type high-pressure apparatus. The crystal symmetry by single-crystal X-ray diffraction analysis is hexagonal, space group $P6_3/m$ (No. 176), with $a = 9.3142(5)$ Å, $c = 6.7010(4)$ Å, $Z = 1$. Gadolinium and Ho are disordered over the two large cation positions, $A(1)$ and $A(2)$, and charge balance in this silicate apatite is maintained by cation vacancies in $A(1)$. Two other apatite-structure crystals investigated have $P\bar{3}$ and $Imma$ symmetry, and represent either partially ordered Gd–Ho distributions or crystal strain induced during quenching.

© 2006 Elsevier Inc. All rights reserved.

1. Introduction

Apatites have long been the subject of scientific investigation because of their potential application in the biomedical sciences [1]. Apatites are a diverse class of materials with a complicated structural chemistry and wide variety of structures and bonding types [2]. The general formula can be described as $A_{10}(TO_4)_6X_2$ with A generally being a large divalent cation (e.g., Ca^{2+}, Sr^{2+}, Pb^{2+}), TO_4 a trivalent anionic group (e.g., PO_4^{3-}, VO_4^{3-}), and X a monovalent anion (e.g., F^-, OH^-, Cl^-) [3–5]. Apatites usually crystallize in the hexagonal $P6_3/m$ space group or one of its subgroups [6,7]. The apatite framework is built up of isolated TO_4^{n-} tetrahedra with the large A^{m+} cations located in two sites, $A(1)$ 9-coordinated and $A(2)$ 7-coordinated. The apatite structure is highly tolerant to cation and anion substitution; for instance, it is possible to substitute divalent calcium by monovalent (e.g. Na^+) or a trivalent cation (e.g., La^{3+}), if the charge is balanced by substitution of the trivalent phosphate group for a divalent

(e.g., SO_4^{2-}) or tetravalent (e.g., SiO_4^{4-}, GeO_4^{4-}) group, respectively [8–11]. Of great interest is the existence of the channel formed by the $A(2)$ cations, running along the c-axis in apatite type structures, which accommodates a column of X anions. Depending on their size and configuration, the X anions are situated at different positions with the $A(2)$ cations arranged in a tricluster around them.

Rare earth (RE)-based apatites have recently attracted considerable attention for their high oxide ion conductivities which make them potentially useful as electrolytes for intermediate-temperature solid oxide fuel cells [12–16]. There are two kinds of RE-based apatite that possess higher conductivities, including the oxygen-excess RE-based silicates and germanates ($La_{10}Si_6O_{27}$ and $La_{10}Ge_6O_{27}$) [17,18] and the cation-deficient RE silicate apatites [19]. Detailed investigations of these compounds have shown that cation nonstoichiometry and partial occupancy of these sites can have as great an affect on conductivity as the incorporation of excess oxygen into the system [20–22]. Furthermore, knowledge of the ionic transport properties of apatite compounds is very important for us to understand their physical and chemical properties. Bouhaouss

---

*Corresponding author. Fax: +86 0431 5168316.
E-mail address: liuxy@jlu.edu.cn (X. Liu).

et al. [23] have investigated the mechanism of ionic conduction in oxy- and hydroxylapatite structures and found that charge-carrying protons should be responsible for the observed conductivities in hydroxylapatite and the H^+ migration between the electroattractive ion (O^{2-}) to give molecular H_2O in matrix channels. In a recent theoretical investigation, Tolchard et al. [24] suggested two pathways of oxide ion conduction for $La_{9.33}(SiO_4)_6O_2$; one is the linear pathway running through the so called "apatite channel" and the other is a non-linear "sinusoidal-like" pathway also running inside the hexagonal channel. In the present work, we report the single crystal synthesis and structure characterization of a double *RE* silicate hydroxyapatite $Gd_{4.33}Ho_{4.33}$ $(SiO_4)_6(OH)_2$, which has a high proportion of cation vacancies in its structure and is potentially a good ionic conductor.

2. Experiment

2.1. Synthesis experiment

The single crystal of the title compound was prepared by direct reaction of stoichiometric amounts of RE_2O_3 (Gd_2O_3, Aldrich, 99.9%; Ho_2O_3, Aldrich, 99.9%) and amorphous SiO_2 (Alfa Aesar, 99.999%) in the presence of $\sim$10–11 wt% distilled water at 2.0 GPa, 1450 °C for 12 h in a piston-cylinder-type apparatus. Pressure was calibrated from melting of dry NaCl at 1050 °C [25] and the transformation of quartz to coesite at 500 °C [26]. All the furnace parts were previously fired at 1000 °C in air. The experimental temperature was monitored by inserting a Pt100%–Pt90%Rh10% thermocouple into the high-pressure cell. The starting mixture was encapsulated in a sealed platinum tube with a diameter of 5 mm and a height of 8 mm, which was separated by MgO powder from a graphite heater. The experiment was quenched before the pressure was released.

The product of our high-pressure synthesis was characterized by means of optical polarizing microscopy, and powder and single-crystal X-ray diffraction (XRD). The composition of the product was analyzed by a JEOL 8600 Superprobe, which was operated at an accelerating voltage of 20 kV, a beam current of 15 nA, a beam diameter of 2 μm, and 20 s counts, using $HoPO_4$, $GdPO_4$, and albite ($NaAlSi_3O_8$) as standards, and the measurements were reduced using the Love–Scott model [27]. A scanning electron microscope (SEM) image and electron probe X-ray microanalysis (EPMA) are shown in Fig. 1 and Table 1, respectively. From the SEM photographs (Fig. 1) we can clearly see that there exist two distinct phases in the product with different brightness, bright and dark, corresponding to *RE* silicate hydroxyapatite, and an unidentified *RE* disilicate, respectively.
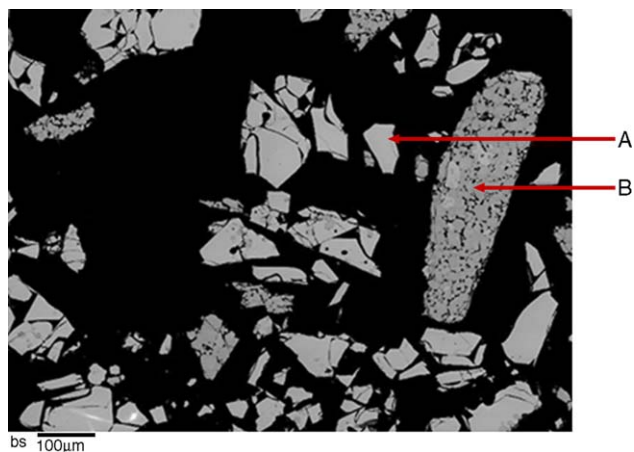

Fig. 1. SEM photograph of the experimental product: (A) the bright phase (Gd–Ho silicate hydroxyapatite) and (B) the dark phase (Gd–Ho disilicate).

Table 1
Composition of experimental products

	Ho	Gd	Si	O
Bright phase	0.85	0.87	1.28	6
Dark phase	0.99	1.03	2.00	7

2.2. X-ray structures

We selected three single crystals of the title compound for single-crystal X-ray analysis, using optical polarizing microscopy. Single-crystal fragments were reduced in size and shaped by trimming with a scalpel blade, and evaluated for X-ray structure analysis by optical petrography and X-ray precession photography and diffractometry. Single-crystal measurements were made at room temperature and pressure with a Bruker Kappa CCD diffractometer and graphite-monochromatized MoKα X-radiation (50 kV, 32 mA, $\lambda = 0.71069$ Å). The COLLECT Nonius software was used for unit-cell refinement and data collection. The reflection data were processed with SORTAV-COLLECT, using an empirical procedure for absorption correction, and SHELXTL/PC [28] and Fourier methods were used for structure determination. Structure refinements were made with LINEX77 (State University of New York at Buffalo), using scattering factors for neutral atomic species and values of f' and f'', respectively, from Tables 2.2A and 2.3.1 of the *International Tables for* X-ray *Crystallography* [29]. Final parameters and other relevant experimental details of the bright (apatite) phase are given in Tables 2 and 3, and selected bond distances and angles in Table 4. Unfortunately, the dark phase was present only as massive aggregates of crystals that were too small for conventional-source X-ray structure analysis.

Table 2
Atomic coordinates (Å) and equivalent isotropic displacement parameters (Å^2) for double RE silicate hydroxyapatite [Gd$_{4.33}$Ho$_{4.33}$(SiO$_4$)$_6$(OH)$_2$]

Atom	Site occupancy	X	y	z	U_{eq}
A(1)	0.671(3)	2/3	1/3	0.9969(2)	0.0145(8)
A(2)	0.997(1)	0.99225(8)	0.23355(8)	1/4	0.0131(3)
Si	1.0	0.3758(5)	0.4024(4)	1/4	0.0092(8)
O(1)	1.0	0.4924(11)	0.3234(12)	1/4	0.019(2)
O(2)	1.0	0.4700(12)	0.5976(11)	1/4	0.029(3)
O(3)	1.0	0.2530(9)	0.3425(11)	0.0615(11)	0.042(3)
O(4)	0.5	0	0	0.217(4)	0.012(5)[a]
H	0.5	0	0	0.07	0.012[b]

Experiment JLU011; crystal—0.020 × 0.080 × 0.100 mm^3, equant; $a = 9.3142(5)$, $c = 6.7010(4)$ Å; space group $P6_3/m$; reflections—534 unique, 231 with $I < 3\sigma$, $R_{int} = 0.053$; $R = 0.038$; w$R = 0.031$; $s = 2.004$; $\Delta\rho = +2.19$, -2.84 eÅ^{-3}; $U_{eq} = (1/3)\Sigma_i\Sigma_j U^{ij}a^i a^j a_i a_j$.
[a] Isotropic refinement.
[b] Not refined; $A = $ Gd + Ho.

Table 3
Anisotropic displacement parameters (U_{ij}, Å^2)[a] and bond valences (s)[b]

Position	U_{11}	U_{22}	U_{33}	U_{12}	U_{13}	U_{23}	s
A(1)[c]	0.0137(8)	0.0137(8)	0.0159(8)	0.0069(8)	0.0	0.0	3.14
A(2)	0.0128(4)	0.0152(4)	0.0114(4)	0.0071(3)	0.0	0.0	2.94
Si	0.009(2)	0.010(2)	0.008(2)	0.005(2)	0.0	0.0	4.36
O(1)	0.011(5)	0.030(6)	0.022(6)	0.014(5)	0.0	0.0	2.24
O(2)	0.019(6)	0.013(5)	0.053(9)	0.006(5)	0.0	0.0	2.37
O(3)	0.036(5)	0.098(7)	0.014(4)	0.051(5)	0.0	0.0	2.08
O(4)	—	—	—	—	—	—	2.72
H	—	—	—	—	—	—	0.87

[a] Anisotropic temperature factors have the form exp[$-2\pi^2(U_{11}h^2a^{*2} + \cdots + 2U_{23}klb^*c^*\cos\alpha^*)$].
[b] Bond valence parameters [41].
[c] $A = $ Gd + Ho.

Table 4
Bond distances (Å) and angles (°) in Gd$_{4.33}$Ho$_{4.33}$(SiO$_4$)$_6$(OH)$_2$

A(1)–O(1)	× 3	2.317(6)	O(4)-H		1.0[a]
A(1)–O(2)^I	× 3	2.365(7)			
A(1)–O(3)^I	× 3	2.751(9)	Si–O(1)		1.587(10)
Mean		2.478	Si–O(2)		1.574(10)
			Si–O(3)	× 2	1.605(8)
A(2)–O(1)		2.690(9)	Mean		1.593
A(2)–O(2)^{II}		2.394(10)			
A(2)–O(3)	× 2	2.260(7)	O(1)–Si–O(2)		114.8(6)
A(2)–O(3)^{III}	× 2	2.461(7)	O(1)–Si–O(3)	× 2	111.9(3)
Mean		2.421	O(2)–Si–O(3)	× 2	106.9(4)
			O(3)–Si–O(3)^{IV}		103.8(6)
A(2)–O(4)		2.223(3)	Mean		109.4

$A = $ Gd + Ho.
Symmetry codes. I: $-x$, $-y$, $-z$; II: $1 + (y-x)$, $-x$, z; III: $1 + x$, y, z; IV: x, y, $0.5-z$.
[a] Not refined.

3. Results and discussion

3.1. Phase analysis

The results of the SEM and EPMA studies (Table 1; Fig. 1) show that there are two phases in our experimental product. According to the EPMA result, we believe that the dark phase is a previously unreported double RE disilicate. The powder XRD pattern of our experimental apatite product is shown in Fig. 2(a). It is generally in good agreement with the calculated XRD pattern for Gd$_{4.33}$Ho$_{4.33}$(SiO$_4$)$_6$(OH)$_2$, based on the present single
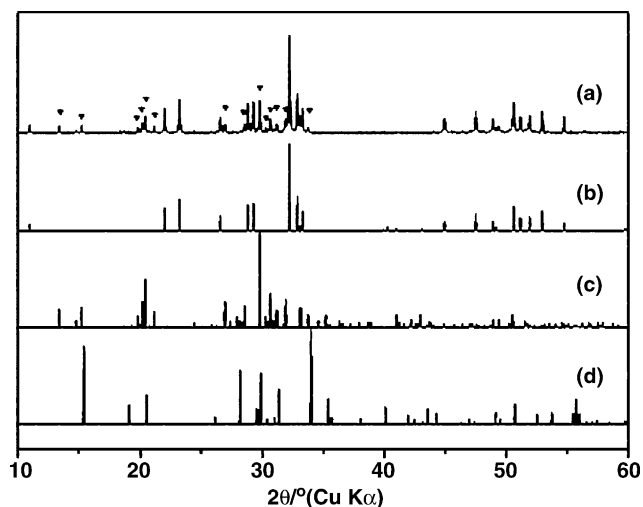
Fig. 2. (a) Experimental XRD patterns of product; (b) calculated XRD powder patterns of the title compound; (c) calculated XRD patterns of type B holmium disilicate ($Ho_2Si_2O_7$) and (d) calculated XRD patterns of type X lutetium disilicate ($Lu_2Si_2O_7$).

Fig. 3. Crystal structure of double RE hydroxyapatite $Gd_{4.33}Ho_{4.33}$ $(SiO_4)_6(OH)_2$ along [001] direction. $RE(2)$ atoms define the apatite channel and are, in turn, enclosed by a hexagon of $RE(1)$.

crystal structure analysis [Fig. 2(b)], except that there are a small number of additional weak peaks, which are denoted by triangles and represent contamination by the dark phase. To help characterize the dark phase RE disilicate, we have also calculated the powder XRD patterns of holmium disilicate ($Ho_2Si_2O_7$, type B) and lutetium disilicate ($Lu_2Si_2O_7$, type X) based on their single crystal structures, which are reported by Fleet and Liu [30,31], as shown in Fig. 2(c) and (d), respectively. Through comparison of peak positions and intensities, we conclude that the dark phase in our product is more like the type B RE disilicate.

From the work of Fleet and Liu [9,30–32], we know that the presence ~3–5% water invariably induces the synthesis of RE disilicate. Therefore, we believe that the simultaneous appearance of double RE disilicate and double RE silicate hydroxyapatite in our product is attributable to the heterogeneous distribution of H_2O in the capsule. The two phases in our product must have been synthesized in different areas in the capsule. The H_2O-rich part in the center of the capsule led to the formation of double RE silicate hydroxyapatite and the double RE disilicate was formed nearby the capsule wall.

3.2. Double RE silicate hydroxyapatite

Structure analysis reveals that the title compound crystallizes in the usual apatite space group $P6_3/m$ with $a = 9.3142(5)$ Å, $c = 6.7010(4)$ Å, $Z = 1$. The two other apatite-structure crystals investigated gave trigonal $P\bar{3}$ symmetry with $a = 9.3140(7)$ Å, $c = 6.7004(4)$ Å and orthorhombic $Imma$ symmetry with $a = 13.3950(6)$ Å, $b = 16.1311(8)$ Å, $c = 9.3129(6)$ Å, but did not yield satisfactory structures. These two crystals were either partially ordered in respect to Gd–Ho distributions or
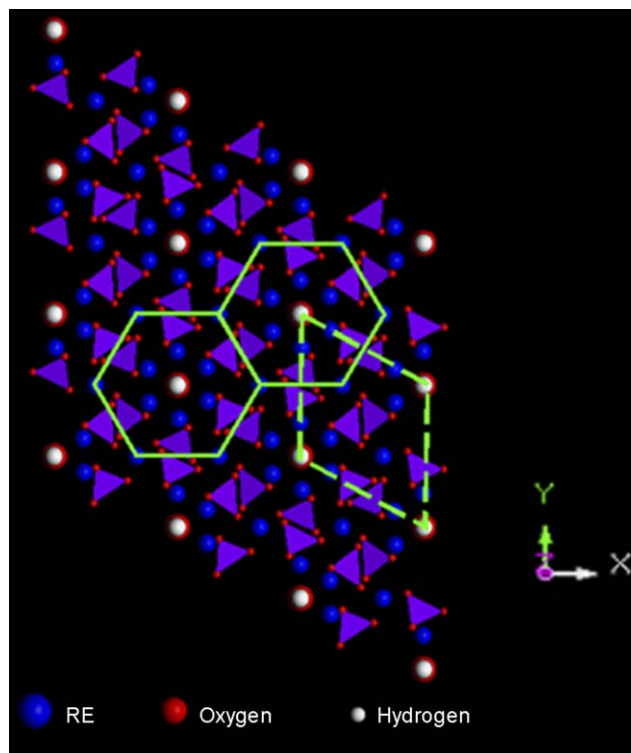
strained during quenching. The cell volume of the title compound is decreased slightly compared with $La_{9.33}$ $(SiO_4)_6O_2$ [33]: this is attributable to a decrease in the mean ionic radius of the RE^{3+} cation and the high proportion of vacancies in the $RE(1)$ position. The crystal structure (Figs. 3 and 4) is built from an isolated SiO_4 tetrahedron and two different kinds of REO_n ($n = 7$, 9) polyhedra. The Si–O distances range from 1.574 to 1.605 Å (mean 1.593 Å), and the O–Si–O bond angles from 103.8° to 114.8° (mean 109.4°), respectively (Table 4). $RE(2)$ cations form hexagonally shaped channels along the [001] direction, which are surrounded by six columns of $RE(1)$ cations (Fig. 3). Because of their nearly identical chemical character, Gd and Ho should distribute randomly in $A(1)$ and $A(2)$ sites in the title compound with the ratio 1:1, and the charge-balanced formula of $Gd_{4.33}Ho_{4.33}(SiO_4)_6(OH)_2$. The $RE(1)$ atoms are connected to nine oxygen atoms with $RE(1)$–O bond distances ranging from 2.317 to 2.751 Å (mean 2.478 Å) and the $RE(2)$ atoms are connected to seven oxygen atoms with the $RE(2)$–O bond distances ranging from 2.223 to 2.690 Å (mean 2.393 Å). All bond distances and RE site occupancies are consistent with the literature studies of RE silicate apatites [8,9,19,34–38]. The point symmetries at $RE(1)$ and $RE(2)$ sites are C_3 and C_1, respectively, showing that the later is the more distorted cation site.

The oxygen anion in the apatite channel [O(4)] is located on the 6_3 axis and coordinated with three $RE(2)$ cations
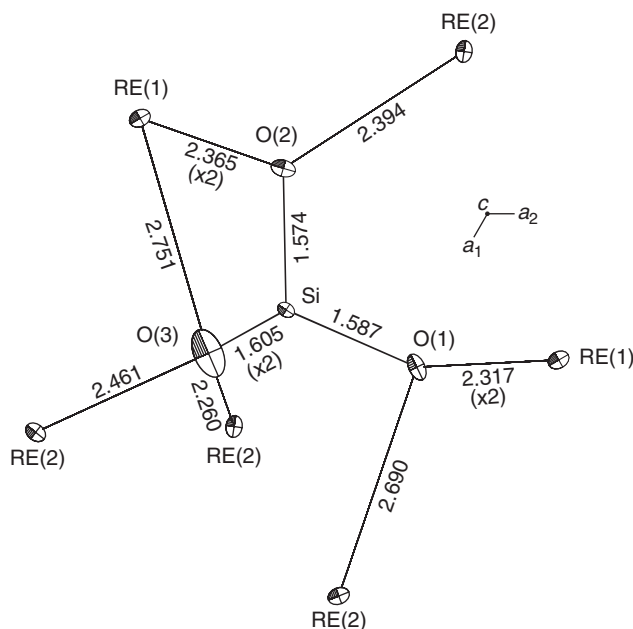
Fig. 4. Bond distances (Å) and anisotropic displacement in $Gd_{4.33}Ho_{4.33}$ $(SiO_4)_6(OH)_2$: note that the exaggerated anisotropic displacement of O(3) is attributable to the high proportion of vacancies in RE(1) and near-equatorial distribution of strong bonds to Si and RE(2).

arranged in a tricluster perpendicular to the c-axis. An isotropic displacement parameter was used for O(4), and the H atom was assumed to ride on it. The OH^- anions are stacked in a regular column in the apatite channel and, in the locally ordered structure, their polar direction is flipped in neighboring channels [39]. However, the mirror plane at $z = 1/4$ indicates domain disordering of the hydroxyl group and results in O(4) and H occupancies of 0.5. As mentioned in the Introduction, because of their difference in size, the channel (X) anions are situated at different heights (z) in the various apatite end-member compounds, and modulated structures exist for hydroxyl and chlor end-members and solid solutions [40]. The O(4) anion is located at $z = 0.217$ in this study; small differences with the ideal hydroxyapatite structure are attributed to difference in ionic radius between Ca^{2+} and RE^{3+}. The presence of the OH group, characterizing the apatite as Gd–Ho silicate hydroxyapatite, was confirmed by comparing refinements of the hypothetical oxyapatite $[RE_{9.33}(SiO_4)_6O_2]$ and the present hydroxyapatite $[RE_{8.67}(SiO_4)_6(OH)_2]$ structures. The oxyapatite formula resulted in an inferior refinement: R and wR were increased to 0.041 and 0.036, respectively, and the occupancy of RE(2) exceeded unity (1.073, compared with 0.997 for the hydroxyapatite structure). Moreover, the difference electron density map calculated for the hydroxyapatite structure with O(4) and H omitted revealed residual electron density at H which was very close to one-eighth of that at O(4). The bond valence for O(4) bonded to H and the tricluster of $RE(2)^{3+}$ cations is significantly greater than 2 (2.72; Table 3), but most of the other bond valences exceed expected values as well because of the high proportion of vacancies (about 33%) in RE(1).

Although the conductivity of $Gd_{4.33}Ho_{4.33}(SiO_4)_6(OH)_2$ has not been measured because of the impure nature of our product, the high proportion of cation vacancies in RE(1) sites suggests that this apatite might be a good candidate for an ionic conductor.

4. Conclusion

A double RE silicate $Gd_{4.33}Ho_{4.33}(SiO_4)_6(OH)_2$ with the hydroxyapatite structure has been synthesized at 2.0 GPa and 1450 °C using a piston-cylinder high-pressure apparatus. The two RE cations are distributed randomly amongst the A(1) and A(2) sites, and charge balance is maintained by cation vacancies in A(1). The presence of two different RE cations in the same compound might promote a better understanding of the co-operative effects of ions under solid-state conditions.

Acknowledgments

References

[1] T.S.B. Narasaraju, D.E. Phebe, J. Mater. Sci. 31 (1996) 1.
[2] D. McConnell, Apatite, Springer, Wien, New York, 1973.
[3] H.E. Feki, J.M. Savariault, A.B. Salah, J. Alloys Compd. 287 (1999) 114.
[4] T. Naddari, J.M. Savariault, H.E. Feki, P. Salles, A.B. Salah, J. Solid State Chem. 166 (2002) 237.
[5] H.P. Beck, M. Douiheche, R. Haberkorn, H. Kohlmann, Solid State Sci., in press.
[6] P.E. Mackie, J.C. Elliot, R.A. Young, Acta Crystallogr. B 28 (1972) 1840.
[7] T.J. White, D. Zhili, Acta Crystallogr. B 59 (2003) 1.
[8] M. Takahashi, K. Uematsu, Z.G. Ye, M. Sato, J. Solid State Chem. 139 (1998) 304.
[9] M.E. Fleet, X.Y. Liu, J. Solid State Chem. 178 (2005) 3275.
[10] T. Nakajima, K. Nishio, T. Ishigaki, T. Tsuchiya, J. Sol–Gel Sci. Technol. 33 (2005) 107.
[11] A. Piotrowski, V. Kahlenberg, R.X. Fischer, J. Solid State Chem. 163 (2002) 398.
[12] S. Nakayama, T. Kageyama, H. Aono, Y. Sadaoka, J. Mater. Chem. 5 (1995) 1801.
[13] S. Nakayama, M. Sakamoto, J. Eur. Ceram. Soc. 18 (1998) 1413.
[14] S. Nakayama, M. Sakamoto, M. Higuchi, K. Kodaira, T. Suzuki, K. Itoh, J. Eur. Ceram. Soc. 19 (1999) 507.
[15] S. Nakayama, M. Sakamoto, M. Higuchi, K. Kodaira, J. Mater. Sci. Lett. 19 (2000) 91.
[16] M. Higuchi, Y. Masubuchi, S. Nakayama, S. Kikkawa, K. Kodaira, Solid State Ionics 174 (2004) 73.
[17] H. Arikawa, N. Nishiguchi, T. Ishihara, Y. Takita, Solid State Ionics 31 (2000) 136.
[18] S. Tao, J.T.S. Irvine, Mater. Res. Bull. 36 (2001) 1245.
[19] J.E.H. Sansom, D. Richings, P.R. Slater, Solid State Ionics 139 (2001) 205.
[20] J.E.H. Sansom, L. Hildebrandt, P.R. Slater, Ionics 8 (2002) 155.
[21] J.E.H. Sansom, P.R. Slater, Solid State Phenom. 90–91 (2003) 189.
[22] J. MacFarlane, S. Barth, M. Swaffer, J.E.H. Sansom, P.R. Slater, Ionics 8 (2002) 149.

[23] A. Bouhaouss, A. Laghzizil, A. Bensaoud, M. Ferhat, G. Lorent, J. Livage, Int. J. Inorg. Mater. 3 (2001) 743.
[24] J.R. Tolchard, M.S. Islam, P.R. Slater, J. Mater. Chem. 13 (2003) 1956.
[25] S.R. Bohlen, Neues Jb. Mineral. Mh. 9 (1984) 404.
[26] S.R. Bohlen, A.L. Boettcher, J. Geophys. Res. 87 (1982) 7073.
[27] D.A. Sewell, G. Love, V.D. Scott, J. Phys. D 18 (1985) 1233.
[28] Siemens: SHELXTL PC (Version 4.1). Siemens Analytical X-ray Instruments, Inc., Madison, WI 53719, USA, 1993.
[29] J.A. Ibers, W.C. Hamilton (Eds.), International Tables for X-ray Crystallography, vol. IV, Kynoch Press, Birmingham, UK, 1974.
[30] M.E. Fleet, X.Y. Liu, J. Solid State Chem. 161 (2001) 166.
[31] M.E. Fleet, X.Y. Liu, Z. Kristallogr. 218 (2003) 795.
[32] M.E. Fleet, X.Y. Liu, Am. Mineral. 89 (2004) 396.
[33] H. Okudera, Y. Masubuchi, S. Kikkawa, A. Yoshiasa, Solid State Ionics 176 (2005) 1473.

[34] J. Felsche, J. Solid State Chem. 5 (1972) 266.
[35] J.M. Hughes, A.N. Mariano, J.W. Drexler, Neues Jb. Mineral. Mh. (1992) 311.
[36] D.C. Noe, J.M. Hughes, A.N. Mariano, Z. Kristallogr. 206 (1993) 233.
[37] P. Berastegui, S. Hull, F.J. GarcíaGarcía, J. Grins, J. Solid State Chem. 168 (2002) 294.
[38] L. León-Reina, M.C. Martí-Sedeňo, E.R. Losilla, A. Cabeza, M. Martíez-Lara, S. Bruque, F.M.B. Marques, D.V. Sheptyakov, M.A.G. Aranda, Chem. Mater. 15 (2003) 2099.
[39] S. Peroosa, Z. Dub, N.H. de Leeuwa, Biomaterials 27 (2006) 2150 and references therein.
[40] K. Sudarsanan, R.A. Young, A.J.C. Wilson, Acta Crystallogr. B 33 (1977) 3136.
[41] N.E. Brese, M. O'Keeffe, Acta Crystallogr. B 47 (1991) 192.